Spontaneous spirals in vibrated granular chains

R. E. Ecke[1,2], Z. A. Daya[1,2], M. K. Rivera[1,2], and E. Ben-Naim[1,3]
[1] *Condensed Matter & Thermal Physics Group,* [2] *Center for Nonlinear Studies,* [3] *Theoretical Division*
Los Alamos National Laboratory, Los Alamos, NM 87545

We present experimental measurements on the spontaneous formation of compact spiral structures in vertically-vibrated granular chains. Under weak vibration, when the chain is quasi two-dimensional and self-avoiding, spiral structures emerge from generic initial configurations. We compare geometrical characteristics of the spiral with that of an ideal tight spiral. Globally, the spiral undergoes a slow rotation such that to keep itself wound, while internally, fast vibrational modes are excited along the backbone with transverse oscillations dominating over longitudinal ones. Spirals have an extremely small volume in phase space, and hence, their formation demonstrates how nonequilibrium dynamics can result in a nonuniform sampling of phase space.

PACS numbers: 81.05.Rm,83.10Nn

I. INTRODUCTION

Ratchet mechanisms are thought to play an important role in producing net transport or motion by asymmetrically absorbing energy from a stochastic source [1–4]. Such mechanisms should apply to systems far from equilibrium as well, specifically with respect to the formation of patterns or structures. In other words, spontaneously generated patterns might arise from a stochastic forcing. Shaken granular media are natural systems for investigating possible ratchet effects in nonequilibrium systems [5]. Mechanical vibration is athermal and coupled with the dissipative collisions results in effectively a stochastic forcing often manifested by anomalous velocity fluctuations [6–8].

Recently, we have explored a chain of coupled hollow spheres attached by rods and vibrated vertically on a horizontal surface [9,10]. The vertical vibration pumps energy into the chain and, because the collisions with the plate are typically asynchronous with the drive, the chain develops irregular vertical structure. Collisions between balls on the chain generate a noisy dynamics of lateral motions so that viewed from above the chain appears as effectively two-dimensional. Further, when the vibration is weak so that the vertical displacement of the chain is less than one ball diameter, the chain cannot cross itself and is self-avoiding.

Previous experiments suggest that vibration induces strong fluctuations which in turn cause the chain to explore all regions of the available phase space, similar to the ergodicity principle in equilibrium statistical mechanics. Statistical properties of the unraveling times of knots is consistent with random thermal motion of the crossing points constituting the knot [9]. Moreover, two-loop figure-eight configurations in a ring chain prefer states with maximal disparity in the size of the loops, consistent with uniform sampling of the microscopic configuration space [10]. Further, the statistical properties of free and closed chains [11,12] are reminiscent of the properties of ideal polymers in equilibrium systems [13,14] for such quantities as, for example, the radius of gyration.

One would expect on the basis of these previous results that a free chain weakly excited so that it cannot cross itself would explore phase space uniformly. Such is not the case. Instead the chain may form a compact spiral, see Figure 1a, starting from some generic initial condition. From the available phase space, the system condenses into a very small region, namely the spiral state. In this paper, we present a characterization of the spiral state. We start with a short description of the experimental apparatus, followed by discussions of the formation, geometry and dynamics of the spirals.

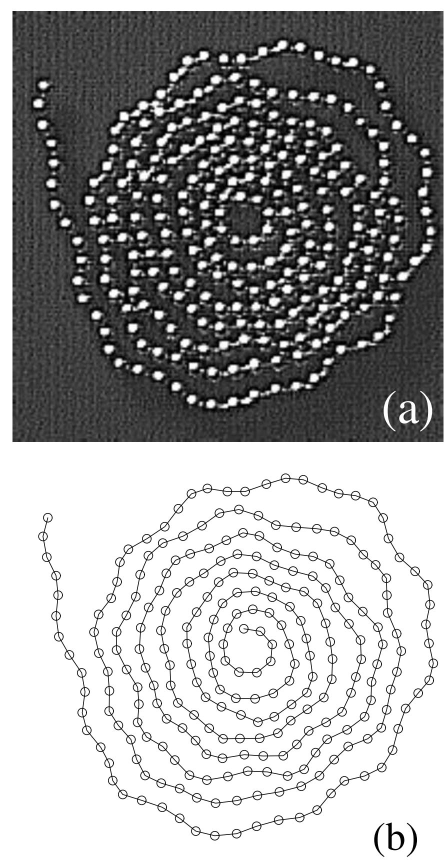

FIG. 1. The raw image (a) and the reconstructed spiral (b).

II. EXPERIMENTAL SET-UP

The experiment consists of a vertically-vibrated anodized-aluminum plate driven harmonically by an electromagnetic shaker. The plate was circular with a diameter of 11.50 inches. It was coupled to the shaker by a shaft that occupied the bore of a precise square-section linear air bearing. As a result, the plate's vertical vibration was accurately sinusoidal with amplitude A and angular velocity $\omega = 2\pi f$ where f is the driving frequency. In addition, the square-section of the bearing ensured that the plate did not experience rotational torques. An acrylic lateral boundary confined the chain to the plate. The instantaneous acceleration of the plate, measured with an accelerometer, was maintained at constant value of the dimensionless peak acceleration $\Gamma = a/g = \omega^2 A/g$ to within 2%.

The commercially-available ball chain consisted of N hollow, approximately spherical shells that were connected by dumb-bell shaped rods. The chains were nickel-plated steel with a nominal bead diameter $d = \frac{3}{32}$ inches with a variation of about 1%. The rods had a diameter $0.22d$ and constrained the inter-bead separation $1 \le b \le 1.4$ measured in units of the bead diameter. The maximal angle between two consecutive rods was $\approx 50^\circ$ so that the smallest circle that could be made from the chain had $n = 8$ beads. The ratio of the diameter of the available plate to the bead diameter is about 110, and boundary effects were negligible.

In our experiments, a ball chain was placed onto the vibrating plate. The relevant driving conditions are the frequency, f, and the acceleration, Γ. We restricted our attention to weak vibration, $\Gamma < 2$, where the geometry is quasi two-dimensional. The chain is initiated in a random configuration subject only to the condition that it did not intersect itself. In these weak driving conditions, the chain remains close to the plate surface, free of self-intersections.

We obtained digital images of the chain using a high-resolution (1024 x 1024 pixels) CCD camera. Data sets were acquired at frame rates of 1 Hz to observe the slow global dynamics and at 250 Hz to characterize internal vibrational modes. Using standard image analysis procedures, we extracted positions of the bead centers. These were then ordered to recover the locus of the spiral. For more details see [10]. A typical image and chain reconstruction are shown in Figure 1.

III. SPIRAL FORMATION

We find experimentally that sufficiently long chains spontaneously organize into spirals in a narrow range of accelerations, $1.70 \le \Gamma \le 1.85$, and frequencies $10 \le f \le 25$ Hz. Starting from a linear chain, a tight spiral core nucleates (either clockwise or counter clockwise) at one end of the chain. This core rotates, and as a result the chain winds into a spiral. The formation of compact spirals from a nucleated core typically takes $3-7$ minutes for a chain with $N = 256$ beads. However, the nucleation of the spiral core from a linear chain is a random event occurring on the scale of 30 minutes. Once formed, the spiral was stable.

The formation of spirals is more sensitive to variations in the acceleration rather than in the frequency, similar to pattern formation and clustering in vibrated granular layers [15,16]. When the acceleration is too large, the chain exhibits strong excitations that quickly destroy the spiral. On the other hand, when the acceleration is too small, lateral chain motion is insufficient to nucleate the spiral core.

Interestingly, for a given chain, the spiral always nucleates with its core at the same end. Moreover, artificially formed spirals with their core at the opposite end are unstable. The mechanism responsible for this symmetry breaking are minute imperfections in size, shape, and weight of the extremal beads. Asymmetry underlies numerous transport phenomena in physical and biological systems, for example, Brownian motors [3]. Typically, asymmetry in the environment coupled with oscillatory driving leads to ratchet motion. While similar in spirit, granular chains are different in that the asymmetry is in the transported object itself. Such a transport mechanism may be relevant in biological systems, for example, it can be realized via defects in the macromolecules.

IV. SPIRAL GEOMETRY

The asymmetries are important in the nucleation of the spiral core and its evolution to a compact rotating state. Since we are unable to systematically control these asymmetries, we do not consider here the transient formation stage, but rather, we focus on the characteristics of the formed spiral. As a reference, we use a ideal tight spiral. Consider such a spiral formed by a flexible rope. Without loss of generality, its diameter is set to unity. A point along the spiral is (over)specified by its arc length s, radius r, and winding angle θ. It is convenient to think of the spiral as composed of concentric tori. In such an arrangement, the addition of the outermost torus increases the angle by $\Delta\theta = 2\pi$ and the arc length by $\Delta s = 2\pi r$. Since $\Delta r = 1$ we have $ds/dr = 2\pi r$ and $ds/d\theta = r$. It follows that $r(s) = \sqrt{s/\pi}$ and $\theta(s) = \sqrt{4\pi s}$.

Consider now a bead chain. The bead number n is a natural measure of the arc length, and assuming an average separation of $\langle b \rangle$, one has $s(n) = n\langle b \rangle$. Moreover, the distance between the nth bead and the 1st bead, $r(n)$, is used as a measure of the radius, since the spiral center is not uniquely defined. The (s, θ) coordinates of the first bead are $(1, 0)$. Substituting $s(n) = n\langle b \rangle$ in the above expressions for $\theta(s)$ and $r(s)$, and using the law of cosines yields an expression for the winding angle and distance to the core as a function of the bead number:

$$\theta(n) = \sqrt{4\pi n\langle b\rangle}, \qquad (1)$$

$$r(n) = \sqrt{1 + \frac{n\langle b\rangle}{\pi} - 2\sqrt{\frac{n\langle b\rangle}{\pi}}\cos\theta(n)}. \qquad (2)$$

Of course, these expressions apply to sufficiently large spirals and $n \gg 1$.

We have measured the average angle and distance as a function of the bead number from over 500 frames. In these experiments and for the remainder of this paper we have $N = 256$ beads, $f = 16$ Hz and $\Gamma = 1.77$. In reconstructing the spiral from the image our ordering was such that the innermost core bead corresponds to $n = 1$.

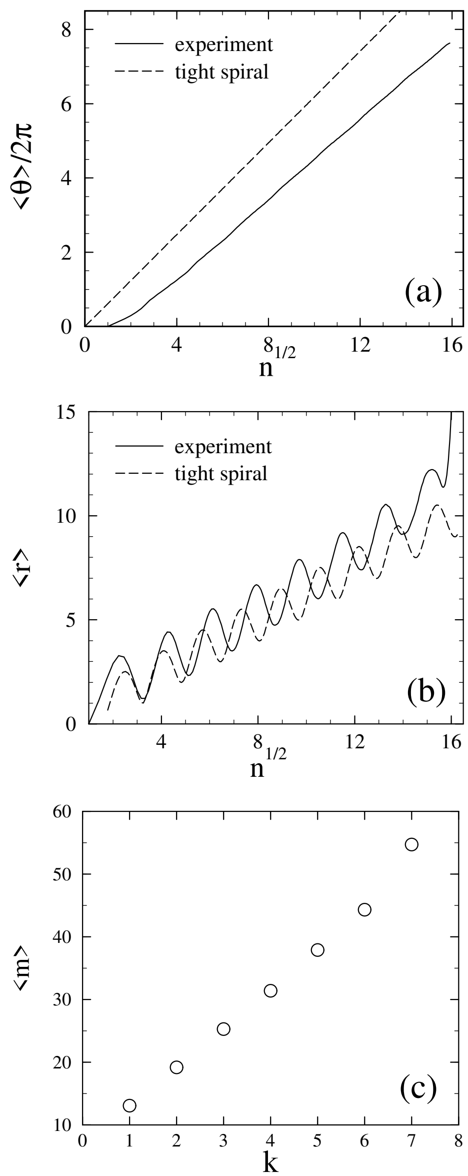

FIG. 2. The mean angle $\langle\theta\rangle/2\pi$ (a) and distance $\langle r\rangle$ (b) as a function of $\sqrt{n}$. In (c) the mean number of beads $\langle m\rangle$ per turn is plotted vs the turn number k.

In Figures 2a and b we have plotted the averages $\langle\theta\rangle(n)/2\pi$ and $\langle r\rangle(n)$ versus $\sqrt{n}$ respectively. For comparison, we also show the tight spiral angle and distance calculated from Equations (1) and (2). Here, the average separation $\langle b\rangle = 1.2$ was measured directly, as discussed below. The slower (faster) linear growth of $\langle\theta\rangle(n)$ ($\langle r\rangle(n)$) corresponds to the spiral becoming less tight the further one goes from the compact core. Nevertheless, the gross features such as the overall linear growth of $\langle r(n)\rangle$ with $\sqrt{n}$, and the periodic corrections, with a period that is fixed in $\sqrt{n}$, indicate that the spiral is approximately tight.

The periodic oscillations of $\langle r(n)\rangle$ allows for a characterization of the number of beads in a given turn of the spiral. A single turn is contained between two consecutive minima in Figure 2b. As shown in Figure 2c, the mean number of beads per turn grows linearly with the loop index, consistent with the expected behavior for concentric tori. The deviation from linearity for the last turn indicates that the spiral has a straight tail. From this measurement, the average size of the tail is estimated at 10, consistent with direct observation. We also find that different sets of 500 images, corresponding to independently formed spirals, are characterized by quantitatively similar mean angle, distance and number of beads per turn as in Figure 2.

When comparing with a tight spiral, we implicitly assumed that the separation between two beads is constant. Direct measurement shows that this is a reasonable assumption as variations in $\langle b\rangle$ are of the order of 10%. However, this deviation has a clear trend. The separation increases as a function of the bead number and it saturates at a value of $\langle b\rangle \approx 1.24$ for $n > 150$.

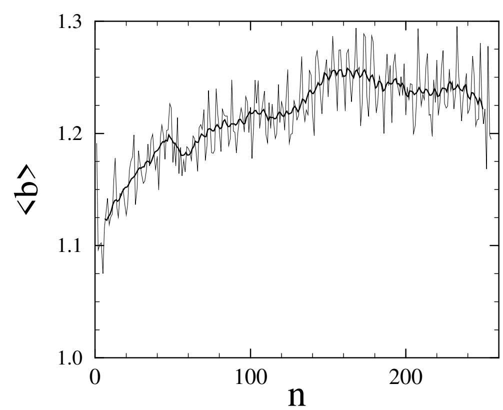

FIG. 3. The average bead separation $\langle b\rangle$ (measured in units of bead diameter d) as a function of the bead number n. The thick line is a 12-bead running average.

V. SPIRAL DYNAMICS

Once formed, the vibrating spiral has dynamics on fast and slow time scales. In Figure 4a, we have plotted an overlay of 16 consecutive reconstructions of the spiral obtained at a sampling rate of 250 Hz. The 16 images correspond to approximately 1 oscillation of the plate.

The lateral wave modes visible here constitute in part the fast dynamics of the spiral. What is not obvious in Figure 4a is the large number of collisions and the constrained motion that effectively gives rise to the transverse modes. Approximately 4 beads separate the nodes of these modes. On a much longer time scale we find that the spiral undergoes axial rotation.

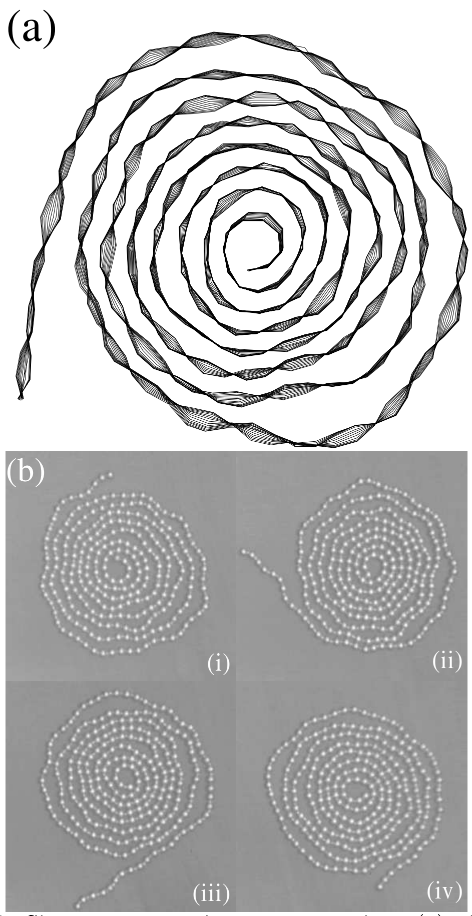

FIG. 4. Sixteen consecutive reconstructions (a) of a spiral during 1 oscillation showing the fast transverse wave modes. Images with a separation of 15 seconds (b) illustrating the slow rotation that keeps the spiral wound.

Four snapshots of a spiral with a separation of 15 seconds or 240 oscillations between snapshots is shown in Figure 4b. The spiral rotates so as to keep tightly wound at a constant rate of about one revolution per minute. On shorter time scales the rotation is not constant, and is better described as a ratcheting motion with the spiral core moving back and forth. The asymmetry between the winding and unwinding motion of the core is transmitted along the spiral length and over long time scales produces the global rotation.

We now focus on the richer fast dynamics. Denoting the displacement in position between consecutive images for each bead $\delta = (\delta_x, \delta_y)$, we find that they are independent of the bead position with slight differences for the end beads. We sampled in excess of 5000 displacements per bead. The data was obtained in sets of approximately 540 frame to frame displacements per experiment sampled at 250 Hz. We verified that for each bead the mean value $\langle\delta\rangle$ vanished and that the displacements were isotropic. Since the spiral rotates, its fast displacements sample all directions in the plane so that the orientation of the coordinate axes is irrelevant. We have plotted the probability distribution functions $P(\Delta_x)$ and $P(\Delta_y)$ in Figure 5. Here, we have defined the normalized displacements $\Delta_{x,y} = \delta_{x,y}/\sigma_{x,y}$ where $\sigma_{x,y}$ are the respective standard deviations. Our results show that the quantities Δ_x and Δ_y are identically distributed with significant incidence for displacements as large as $\pm 3\sigma_{x,y}$. The probability distribution functions are symmetric and non-Gaussian. Over populated (with respect to a Gaussian) velocity distributions [7] and, in particular, exponential tails [8,17] are actually observed in excited granular gases and are understood to be a consequence of the dissipative bead-bead and bead-plate collisions. Our observations suggest that velocity statistics of beads in granular chains may be anomalous as well. Although the exponential tail of the displacement distribution suggests that the velocity distribution has a stretched exponential tail, we are unable to discern its precise form due to insufficient time resolution.

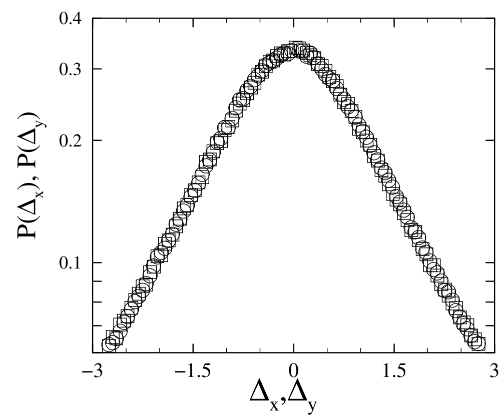

FIG. 5. The probability distribution functions of the normalized displacements Δ_x and Δ_y for all beads of the spiral.

At present we only observe the lateral fast dynamics. The transverse wave modes illustrated in Figure 4b also appear in the vertical plane. Although the in-plane motion consists primarily of transverse modes, they must be accompanied by longitudinal modes that allow for the stretching and contraction of the spiral. To further study these modes we consider the locus of the spiral given by the bead positions $\mathbf{x}_i = (x_i, y_i)$ and inter-connecting rods $\mathbf{r}_i = \mathbf{x}_{i+1} - \mathbf{x}_i$. The mean locus of the spiral $\langle\mathbf{r}\rangle_i$ is defined as the time average of $\mathbf{r}_i(t)$ over an experimental run. For the frame acquired at time t, we calculate the spiral displacements $\Delta\mathbf{r}_i(t) = \mathbf{r}_i(t) - \langle\mathbf{r}\rangle_i$. The longitudinal $L_i(t)$ and transverse $T_i(t)$ displacements from the mean spiral are defined by $\Delta\mathbf{r}_i(t) \cdot \langle\mathbf{r}\rangle_i / |\langle\mathbf{r}\rangle_i|$ and $\Delta\mathbf{r}_i(t) \times \langle\mathbf{r}\rangle_i / |\langle\mathbf{r}\rangle_i|$, respectively. In Figure 6a we have plotted $T_i(t)$ as a function of position and time. The space-time plot shows that between collisions with the plate, positive (negative) displacements continue as positive (negative) *i.e.* the beads are roughly ballistic between collisions. In Figure 6b we plot representative displacements for 80 oscillations of the plate. We see that the transverse displacements are roughly periodic and are significantly larger than the longitudinal ones. This behavior is typical for all interconnecting rods.

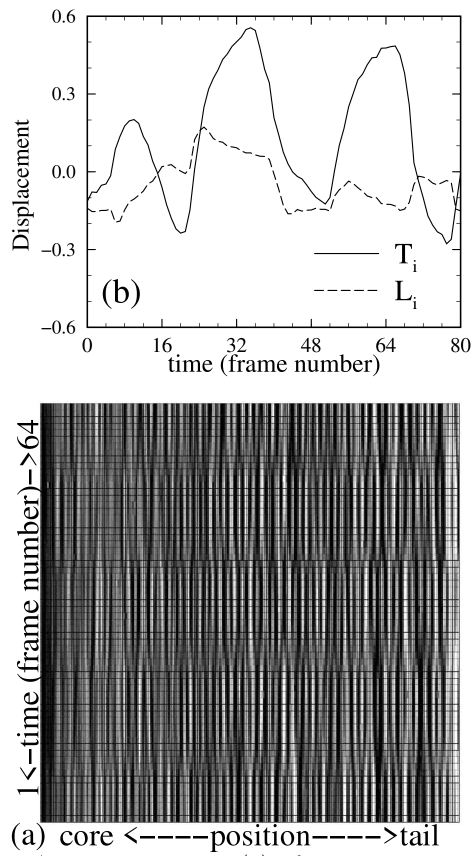

FIG. 6. A space-time plot (a) of the transverse displacements of the spiral. Position (horizontal axis) along the spiral backbone is ordered from core to tail and time (vertical axis) spans 64 consecutive images corresponding to 4 drive cycles. Black (white) denote a positive (negative) displacement. In (b) $T_i(t)$ (solid line) and $L_i(t)$ (dashed line) are plotted for $i = 64$.

VI. CONCLUSION

A general expectation from previous experimental work on granular chains [9–12] is that configurationally the chain assumes very many different states and in this manner explores a large region of its phase space. Contrary to this, we found that a long chain would spontaneously nucleate into a spiral in a narrow range of weak accelerations. It is surprising that a linear chain initiated in a random configuration invariably evolves to a highly specialized state that occupies a very small volume of the available phase space. Moreover, it is interesting that minor differences between the two ends of the chain have such a pronounced effect.

The origins of spiral formation in vibrated chains is the slight forward motion of the chain induced by variations at the ends of the chain. As a result of this asymmetry, the chain crawls forward until it encounters itself. It then has two choices: to turn inwards and wrap itself into a spiral or outwards forming locally aligned chain segments. In the latter case, the end eventually escapes. With successive encounters, it becomes likely that the end will be captured and coil up into a spiral. The rate of nucleation depends, therefore, on the forward ratcheting motion coupled with the possibility of becoming trapped. Such a mechanism would apply to any flexible forward-translating object confined to two-dimensions and moving stochastically.

Once formed, the spiral geometry and dynamics is very reproducible. The spiral becomes looser away from the core and eventually, its tail is practically linear. Dynamically, bead-bead and bead-plate collisions induce transverse and longitudinal modes, the former being stronger. On a longer time scale, the spiral rotates in the direction of coiling and so remains stable.

It will be interesting to further study the spiral formation mechanism. This may be done for example by manipulating one of the chain ends using say a relatively larger bead. Observing the rotation rate as a function of the bead size may elucidate the physical nature of the ratcheting mechanism. Moreover, the nucleation process is in itself intriguing. The distribution of waiting times and its extremal characteristics may alternatively shed light on the same question.

We thank Matthew Hastings, Charles Reichhardt, and James Glazier for useful discussions. This research is supported by the U.S. DOE (W-7405-ENG-36).

---

[1] R. Astumian, Science, **276**, 917 (1997).

[2] F. Julicher, A. Ajdari, and J. Prost, Rev. Mod. Phys., **69**, 1269 (1997).

[3] R.D. Astumian and M. Bier, Phys. Rev. Lett.,**72**, 1766 (1994).

[4] R. Bartussek, P. Hanggi, and J.G. Kissner, Europhysics Letters, **28**, 459 (1994).

[5] I. Derenyi, P. Tegzes, T. Vicsek, Chaos **8**, 657 (1998).

[6] A. Kudrolli, M. Wolpert, and J.P. Gollub,Phys. Rev. Lett.,**78**, 1383 (1997).

[7] F. Rouyer and N. Menon, Phys. Rev. Lett., **85**, 3676 (2000).

[8] J.S. Olafsen and J.S. Urbach, Phys. Rev. E, **60**, R2468 (1999).

[9] E. Ben-Naim, Z.A. Daya, P. Vorobieff, and R.E. Ecke, Phys. Rev. Lett., **86**, 1414 (2001).

[10] M.B. Hastings, Z.A. Daya, E. Ben-Naim, and R.E. Ecke, Phys. Rev. E., **66**, 025102(R) (2002).

[11] Z.A. Daya, M.K. Rivera, E. Ben-Naim, and R.E. Ecke, unpublished.

[12] J.J. Prentis and D.R. Sisan, Phys. Rev. E., **65**, 031306 (2002).

[13] P.G. de Gennes, *Scaling Concepts in Polymer Physics* (Cornell University Press, Ithaca, 1979).

[14] M. Doi and S.F. Edwards, *The Theory of Polymer Dynamics* (Clarendon Press, Oxford, 1986).

[15] B. Umbanhower, F. Melo, and H.L. Swinney, Nature (London) **382**, 793 (1996).

[16] J.S. Olafsen and J.S. Urbach, Phys. Rev. Lett., **81**, 4369 (1998).

[17] X. Nie, E. Ben-Naim, and S.Y. Chen, Europhys. Lett., **51**, 679 (2000)